Research Article

Update for reactive transport modeling of the Kızıldere geothermal field to reduce uncertainties in the early inspections

Selçuk EROL[1],* [ORCID], **Taylan AKIN[2]** [ORCID], **Serhat AKIN[3]** [ORCID]

[1]Energy Systems Engineering Department, Faculty of Engineering, İzmir Institute of Technology, İzmir, Turkey
[2]Geothermal Application & Research Center, Pamukkale University, Denizli, Turkey
[3]Petroleum and Natural Gas Engineering Department, Faculty of Engineering, Middle East Technical University, Ankara, Turkey

Abstract: The development of carbon capture and storage techniques has become essential to reduce and mitigating CO_2 emissions to the atmosphere. CarbFix1 and CarbFix2 projects carried out in Iceland demonstrated that the emissions of waste CO_2 gas from geothermal power plants can be captured and mixed with the effluent geofluid and subsequently injected back into the geothermal reservoir. This experience gained in the CarbFix projects expanded into other geothermal fields around Europe, and one of the demonstration sites is the geothermal field in Turkey, Kızıldere. This paper focuses on the results of an updated study on early field evaluations with reactive transport simulations. In the new three-dimensional numerical model, the geological formations and fault zones were updated according to the well-logs data. Based on the tracer tests performed in the field, the anisotropic permeabilities between the wells were evaluated and imposed into the model. Geofluid chemistry, mineral components, and the volume fractions used as input in the simulations are modified depending on the performed laboratory experiments on the metamorphic schists taken from the geothermal site (i.e. X-ray diffraction (XRD), energy dispersive X-ray (EDX), scanning-electron microscope (SEM), and batch reactor tests). Different thermodynamic databases such as Lawrance Livermore National Laboratory (LLNL) and Thermoddem databases were tested using PHREEQC and TOUGHREACT programs for consistency with experiments. The thermodynamic conditions and the geofluid-rock-CO_2 interactions prevent the mineralization of CO_2 in the reservoir. This outcome differs from CarbFix projects in terms of the carbonization process, but the CO_2 injection is still reliable with solubility-trapping in a geothermal reservoir to partially mitigate the emission. Roughly, 200 kt of CO_2 in 10 years can be safely injected into the geothermal reservoir. According to the new analysis, the ratio of magnesium, sodium, and potassium varies in solid solution series of feldspars and clay minerals as albite end-member and montmorillonite/illite end-members, respectively. The evaluations of solid solution reactions are relatively limited in the law of mass action approach used by PHREEQC and TOUGHREACT.

Key words: Reactive transport, geothermal, CO_2 injection, geofluid-rock interaction

1. Introduction

Carbon storage through geological formations is one of the important methods to mitigate greenhouse gas emissions (Gunnarsson et al., 2018; Topçu et al., 2019). The experiences gained from the Carbfix1 and Carbfix2 projects in Iceland demonstrated that the applicability of carbon storage through mineralization in basaltic geothermal reservoirs is one of the effective techniques to reduce the emissions of coproduced CO_2 from geothermal plants (Snæbjörnsdóttir et al., 2020; Raza et al., 2022). This technique involves capturing CO_2 from geothermal power plants, mixing it with the effluent geofluid, and injecting it into the geothermal reservoir (Aradóttir et al., 2012). In particular, at high enthalpy geothermal reservoir systems, the CarbFix2 was successful with the gas-charged water injection into a hydrothermally altered basaltic reservoir with temperatures around 260 °C (Clark et al., 2020). In the CarbFix2 at the Hellisheiði geothermal power plant in SW Iceland, roughly 25% of the water-soluble gases containing 63 vol% CO_2 were captured from the exhaust of the plant and mixed with the geofluid in a tank at 20 °C. Afterward, the CO_2-charged geofluid was transferred to an injection well to mix with the effluent geofluid in the well before entering the host rock.

In the framework of the Geothermal Emission Control (GECO) H2020 project, the Kızıldere geothermal field in Turkey was one of the demonstration sites for the application of a similar method as CarbFix to metamorphic schist and marble host rocks at a temperature of around 220 °C.

* Correspondence: selcukerol@iyte.gov.tr

In the CarbFix projects, Snæbjörnsdóttir et al. (2018) carried out reaction path modeling to inspect CO_2-geofluid-rock reactions during and after the injection at the CarbFix site at Hellisheidi, SW Iceland. The modeling calculations were modified according to the measured geofluid components at the wellbores. Their study indicated that for CO_2 mineralization in basaltic reservoirs, the suitable conditions are around 5.2 to 6.5 pH at temperatures between 20 °C and 50 °C. Galeczka et al. (2022) further assessed the CO_2 mineralization in basalt at different stages of the process in an extensive range of temperatures from 84 °C to 300 °C with reaction path modeling along the flow path between injection and production wells. In parallel, they performed batch reactor CO_2-geofluid-basalt interaction experiments at different temperatures between 75 °C and 250 °C to validate the modeling calculations. According to their estimation, each tonne of injected CO_2 results in the dissolution of 6.8 m^3 mafic basalt minerals that are olivine or pyroxene, dissociating Mg^{2+}, Ca^{2+}, or Fe^{2+} ions to form secondary carbonate minerals as calcite, dolomite, magnesite, or siderite. The estimated amount of precipitated carbonate minerals is around 7.3 m^3 per injected tone of CO_2. This approximates that 70% of the injected CO_2 can be turned into a solid phase as carbonate minerals below 165 °C. At temperatures between 165 °C and 200 °C, epidote forms as a secondary mineral by consuming Ca^{2+} ions that limit CO_2 mineralization as calcite. Above 200 °C, they evaluated that silicate minerals dominantly consume Mg^{2+}, Ca^{2+}, or Fe^{2+} ions to form secondary minerals which limit the carbonization process.

Ratouis et al. (2021) performed a one-dimensional (1-D) reactive transport simulation to evaluate the CO_2-geofluid-rock interaction in the same geothermal site at Hellisheidi basaltic geothermal reservoir. In the model, several feed zones were determined along the injection wellbore and the corresponding flow paths between injection and production wellbores were created using a 1-D modeling approach. The authors pointed out that at temperatures around 220 to 260 °C, Mg^{2+}, Ca^{2+}, or Fe^{2+} bearing silicates and clay minerals dominantly form as secondary minerals and prevent carbonate mineralization. Moreover, based on the outcomes of these previous studies performed for the same geothermal reservoir, Ratouis et al. (2022) claimed that the fraction of mineralized carbon at the Carbfix demonstration site can be predicted with nonreactive 3-D tracer simulations by assuming natural tracer solutes as boron, and some reactive species such as calcium, and CO_2. The authors used the TOUGH2 simulator (Pruess et al., 1999) with equations of state (EOS1) for tracers which ignore the partial pressure effect of the CO_2 and geochemical interactions. The outcomes were then compared with measured data at the observation wells. The authors believed that the reactive transport simulations, which require extensive computational effort, are not necessary for the verification process of carbon mineralization. As a result, they estimated that 300 Mt of CO_2 can be sequestrated through the flow path by 2050. As Galeczka et al. (2022) mentioned that calcium is a divalent cation that triggers a competitive effect for secondary minerals at a temperature above 165 °C for silicate minerals such as epidote, using calcium as a tracer may lead to misinterpretations. In addition, if the CO_2 goes into the gaseous phase in a real case, this simulator with EOS1 cannot predict two-phase flow (water-CO_2), and it can be challenging to monitor or track the CO_2 as a tracer, particularly, for long-term injection.

Overall, reactive path modeling provides predictions for stagnant conditions to identify secondary species. However, dynamic enthalpy changes along the flow paths between the injection and production wells affect the reactions. Therefore, reactive transport modeling is necessary to take into account transient thermodynamic conditions. In addition, reaction kinetic rates play an important role in the precipitation and dissolution of minerals, particularly carbonates, and these interactions affect the porosity changes of rocks and reactive surface areas of minerals.

In our previous study, we examined preinjection conditions and several injection scenarios and tested various mineral compositions to assess CO_2 carbonization in the Kızıldere geothermal demonstration site with a reactive transport model using the TOUGHREACT program (Erol et al., 2022a). The current study provides an update on the considered geochemical demonstration model of the Kızıldere geothermal field to discard indistinct parameters in the early analysis. Changes from the previous study include the addition of new mineral compositions, geofluid chemistry measured at the laboratory, the fault zones modified based on the well logs, and anisotropic permeabilities for the flow paths between injection and production wells determined based on the tracer tests. Particularly, the Thermoddem thermodynamic database developed by Blanc et al. (2012), in which crystallographic details and constraints are taken into account to delineate pertinent end-members of minerals, considering a solid solution likely occurring within the given system, is implemented and tested.

2. Workflow

Five major steps have been carried out to achieve the evaluation of the CO_2 transport and mineralization reactive process in the geothermal reservoir at the Kızıldere site. Figure 1 demonstrates the workflow for the current study.

Due to the prohibitively extensive computational effort of reactive transport, calibration of pressure-temperature
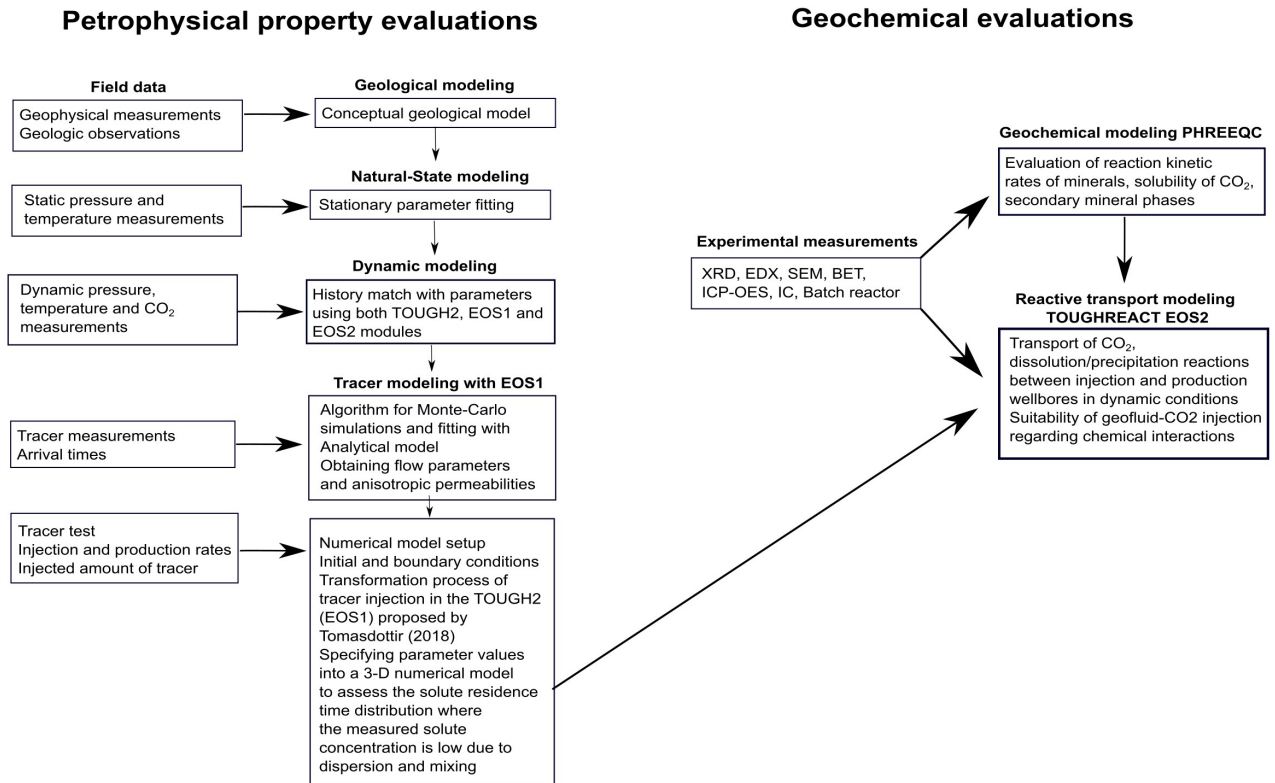
Petrophysical property evaluations   **Geochemical evaluations**

Figure 1. Workflow of the reactive transport simulation for the Kızıldere geothermal reservoir.

(P-T) measurements, tracer fits, and mass fraction of CO_2 is primarily achieved only with heat and mass transfer simulations ignoring the geochemical reaction calculations. Reactive transport is considered in the model after calibration.

The study is carried out with the following procedure:

i) The updated geological structures of the localized Kızıldere field are implemented.

ii) 3-D localized model is run iteratively until P-T and partial pressure of CO_2 distribution reach the natural state conditions of the field (e.g., over 100,000 years). In this step, primarily initial temperature, pressure, and partial pressure gradients, fluxes, and sinks are adjusted.

iii) The production and injection wells are activated for sensitivity analysis with petrophysical properties (anisotropic permeability and porosity values) to obtain the best P-T, the tracer arrival times (TOUGH2-EOS1) and the mass fraction of CO_2 (TOUGH2-EOS2) fits in the dynamic modeling step. In this step, reactive transport is ignored to reduce the computation time. We assumed an equivalent permeability approach.

iv) In addition to field-scale calibration studies, experimental studies were carried out to accurately determine geochemical parameters. Primary and secondary minerals and master chemical species are determined with

X-Ray Diffraction (XRD), energy dispersive X-ray (EDX) with scanning electron microscope (SEM), inductively coupled plasma–optical emission spectrometry (ICP–OES), ion chromatography (IC), and thin section analysis before and after the batch reactor tests. The mineral kinetic constant rates are evaluated by fitting between the measured fluid chemistry and geochemical kinetic reaction-path modeling with the PHREEQC program.

v) When a satisfying match is achieved, the chemical properties, the P-T, mass fraction of CO_2 distribution, and petrophysical properties obtained from steps 2 and 3 are implemented in a model in the TOUGHREACT v1.2 simulator where reactive transport simulation is performed with the production and injection wells. To identify the mineralization process with the maximum CO_2-charged injection, the annual mixing rate is set to 2 kt/year of CO_2 over five years of continuous injection.

The workflow processes and the steps of the study can be seen in Figure 1.

3. Updated numerical model
A 3-D localized reactive transport model is constructed to potentially inject the geofluid-CO_2 into deep metamorphic formation rocks of the geothermal field. The geochemical geofluid-CO_2-rock interaction is scrutinized around the

feed zones of the pilot injection well (Well-G_{inj}) and along with the surrounding flow paths between seven production and three more injection wells in the model (Figure 2).

In the early study, Erol et al. (2022a) constructed the reactive transport model based on the literature data obtained from a field representative of the Kızıldere rock types. The details of the conceptual model, flux boundary conditions, the workflow process for the reactive transport model, and the discussions about the computational cost of the reactive transport simulation, which are similar to those of this model, were elaborated on and delineated in the aforementioned work. After this preexamination, new surveys and analyses carried out in the field provided more details about the fault zones, mineral contents of the reservoir rocks, and arrival times between the wells. Thus, the fault zones are accurately modified concerning the well logs, and the anisotropic permeabilities between the injection and production wells along the fault zones were evaluated with the tracer tests performed in the field and calibrated in the numerical model (Erol et al., 2022b). In this study, based on the previous and recent inspections, we updated the numerical reactive transport model.

The Kızıldere geothermal field is located in the eastern part of Büyük Menderes graben (Alçiçek et al., 2007) and covers a large area for geothermal operations having more than 80 wells. Therefore, the area of interest to be inspected has been localized. Figure 2 shows the numerical model of the localized inspection area in the geothermal field. The concerning heat fluxes, sinks, and sources emerging from the wells located at the outer limits of the localized model boundaries are estimated in a large-scale model and imposed at the boundary blocks of this localized model (Erol et al., 2022a).

3.1. Localized model properties

The new model has 13,584 grid blocks, similar to the previous numerical model but, again, we used a limited block count due to the computational cost of the reactive transport processes. The runtime of a reactive transport simulation is at least three magnitudes larger than a typical heat and flow transport simulation due to iterative chemical equilibration calculation and mass transport, limiting the block count. The Voronoi block area varies from 192 m^2 (volume, 3.6×10^4 m^3) around the wells to 5×10^4 m^2 (volume, 4×10^6 m^3) near the boundaries. The flow paths are created along the fault zones based on the well-log data and the high amount of mud loss during drilling indicating fractures (Figure 2b). The initial permeability and porosity values of corresponding zones are given in Table 1. The shallow reservoir and deep caprocks consist of Pliocene sediments, and metamorphic rocks of the Menderes Massif form the deep reservoir (Şimşek et al., 2005). The provided values are determined based on the tracer test analysis and natural state modeling processes to match with the static P-T measurements. The P-T values are fixed at the top of the model around the depth of 30 m where we need a constraint for the numerical derivations of the flow and partial pressure of CO_2.

The TOUGHREACT v1.2 is used with the Pertasim interface (Xu et al., 2008; Rockware 2022). The reactive
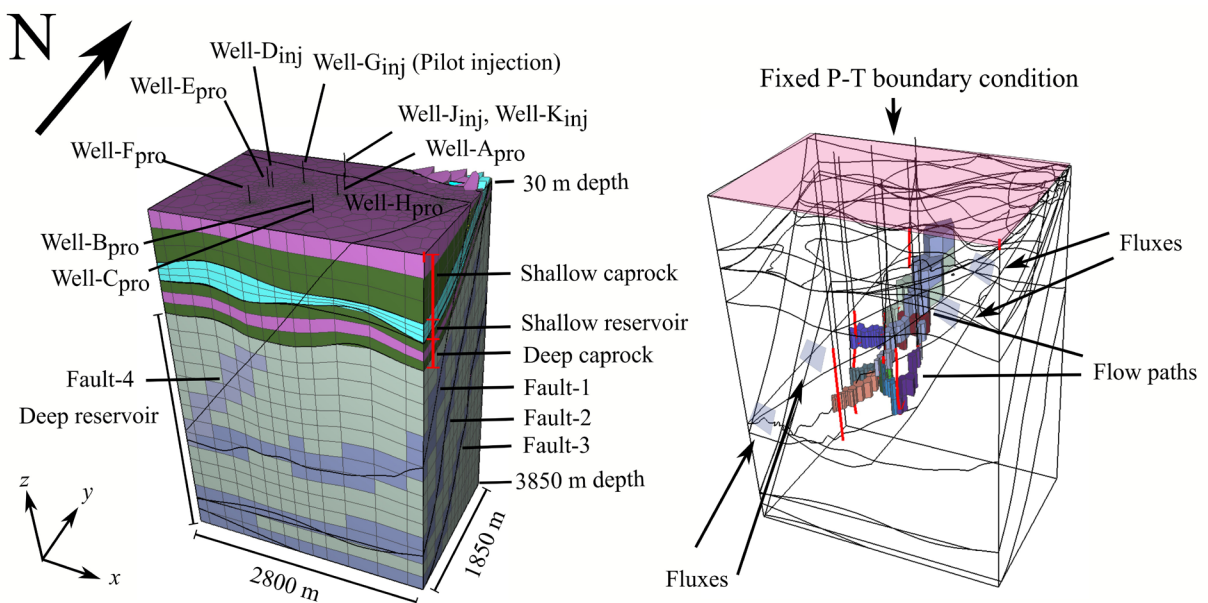

Figure 2. a) Illustration of the localized numerical model with the geological structures and the wells in a localized area of the geothermal field; **b)** Demonstration of the fluxes and boundary conditions in addition to the flow paths between the wells determined based on the tracer arrival times along Fault 2 and crosses to Fault 4. Each flow path between the wells has specific anisotropic permeability values.

Table 1. Permeability and porosity values of the geologic formations and considered flow paths. [a] Based on the tracer test analysis (Erol et al., 2022b).

Zone	XY permeability (m^2)	Z permeability (m^2)	Porosity
Shallow and deep caprocks (violet)	1×10^{-17}	1×10^{-17}	0.01
Threshold zones (green)	1×10^{-16}	1×10^{-16}	0.03
Shallow reservoir (blue) and faults (bluish-gray)	7×10^{-14}	7×10^{-14}	0.04
Matrix domain (gray)	2×10^{-15}	2×10^{-15}	0.03
Flow paths (multicolors in Figure 1b) [a]	1×10^{-11} to 8×10^{-13}	8×10^{-12} to 1×10^{-13}	0.03

transport simulations are coupled with the Equation of State (EOS) module in which water and CO_2 transport processes can be calculated. This EOS, called EOS2, is based on a version of Henry's law correlation developed by Battistelli et al. (1997), which accounts for temperature ranges between 0 °C and 350 °C. In the reactive transport simulations, the solver type is the generalized minimum residual conjugate gradient, and the time step is set to 1 s and automatically changes depending on the geochemical interactions. For convergence, the relative error criterion for the time marching series is specified as 1×10^{-5} (the fully implicit backward Euler).

The mixing ratio of CO_2 is regulated depending on the flow rate of the effluent geofluid (e.g., 50 kg s^{-1}). The effluent geofluid has an ionic strength of 0.12 molality at 105 °C, and the CO_2 partial pressure near the pilot injection well is less than 1 MPa. Therefore, to keep the injection persistent as a single-phase flow, the dissolved CO_2 content in the effluent geofluid should be below 0.1 mol kg^{-1}. The estimated average amount of CO_2 for injection is 2 kt per year (roughly 0.03 mol kg^{-1}). To evaluate the long-term effect of the CO_2 injection in the reservoir, we examined five years of continuous injection. Thus, 2 kt/year of CO_2 is injected as 0.0638 kg s^{-1} that is mixed with 50 kg s^{-1} of effluent geofluid at 105 °C temperature under 1 MPa injection pressure (enthalpy approximately 4.4 $\times 10^5$ J kg^{-1}).

4. Experiments
The cation geofluid chemistry was measured via ICP–OES by Optima 8300 (PerkinElmer 2010; Stefan and Neubauer 2014). The batch reactor, IC, and ICP-OES experiments were performed at International Geothermal Centre (GZB) in Bochum, Germany. The EDX with SEM analyses were carried out at the Ruhr University Bochum with a ZEISS-Gemini2-Merlin high-resolution thermally aided field emission SEM (Berndsen et al., 2022).

Before and after the geofluid-CO_2 injection into the batch reactor, XRD and EDX with SEM analyses are conducted to evaluate the alteration and stoichiometry of the minerals and possible secondary phases.

The volume fraction of primary minerals is determined from the thin section analysis via the box-counting method (Table 2). The reservoir temperature of the Kızıldere geothermal field is typically in the range of 200–220 °C. Since 2018, the pilot injection well is operated with an effluent geofluid temperature of around 105 °C before the CO_2 mixture. The temperature and the flow in the vicinity of the Well-G$_{inj}$ reach pseudo-steady-state conditions. Therefore, a temperature value of around 105 °C is applied for the batch reactor experiments to mimic the test site where the major chemical reactions take place. The experimental evaluations are used to estimate some arbitrary initial guesses of the minerals and for the geofluid chemistry at the reservoir conditions around 220 °C for the simulations and geochemical equilibrium calculations.

The selection of thermodynamic datasets used in the calculations is an ad hoc process, and the different thermodynamic datasets have a significant impact on the results due to the crystallinity degree and/or the compositions of considered mineral phases (Blasco et al., 2017). The equilibrium phases and the rates are calculated with PHREEQC version 3, and the best matches are obtained with the LLNL database (Parkhurst and Appelo, 2013) and Thermoddem database (Blanc et al., 2012). To simulate the mineral alteration and the CO_2-geofluid interactions through the porous medium, the Thermoddem database is imposed in the TOUGHREACT to have a consistent outcome with the experimental evaluations occurring within the given system.

The mineral contents of the examined rock samples are given in Table 2. Approximating nonlinear reactive transport processes at varying P-T conditions are intricate computations, and the definition of the model must be straightforward to avoid convergence problems. Therefore, each rock type is inspected as a different scenario and implemented into two other models to evaluate the possible effects of the geofluid-rock-CO_2 interaction. A summary of the primary and secondary phases used in the reaction transport simulations is provided in Appendix A.

Kinetic rate parameters, as given in Table 3, are estimated by fitting the experimentally measured geofluid chemistry data using the PHREEQC program. The average

Table 2. Mineral contents of the sample.

Rock type	Primary minerals	Secondary minerals
Muscovite-schist	Quartz 58%, muscovite 25%, montmorillonite-Na 13%, hematite 2%, andalusite 1%, paragonite 1%	Albite, calcite, chlorite, dolomite, pyrite, siderite, talc
Quartz-schist	Quartz 91%, muscovite 3%, hematite 2%, andalusite 3%, epidote 1%	Albite, calcite, dolomite, paragonite, pyrite, montmorillonite-Na, siderite, talc

Table 3. Kinetic parameters that are used in reactive transport simulations. [a] Abbreviation is used for names of minerals (Whitney and Evans 2010). [c] Palandri and Kharaka (2004), [d] Based on the sieve analysis.

Minerals	Abb. [a]	Rate constant k_{25} (mol m^2 s^{-1})[b]	The activation energy (kJ mol^{-1}) [c]	Grain size (m) [d]	Average specific surface area (cm^2 g^{-1}) [d]
Albite-low	Ab	2.75×10^{-7}	69	1×10^{-4}	2
Andalusite	And	3×10^{-8}	38	2.5×10^{-4}	2
Calcite	Cal	1×10^{-6}	23	8×10^{-5}	2
Chlorite	Chl	6.4×10^{-17}	16	5×10^{-4}	2
Dolomite (ord)	Dol	2.5×10^{-9}	50	1×10^{-4}	2
Epidote	Ep	1×10^{-12}	70	8.5×10^{-4}	2
Hematite	Hem	2.51×10^{-15}	66	2.5×10^{-4}	1.1
Paragonite	Pg	1×10^{-13}	22	5×10^{-4}	2
Pyrite	Py	2.8×10^{-5}	57	2.5×10^{-4}	1.1
Montmo.-Na	Mnt-Na	1.65×10^{-14}	35	1.5×10^{-5}	11
Muscovite (ord)	Ms	1×10^{-13}	22	4.2×10^{-4}	2
Quartz (alpha)	Qz	2×10^{-14}	77	8.5×10^{-4}	2
Siderite	Sd	1×10^{-9}	50	2.5×10^{-4}	2
Talc	Tlc	1×10^{-12}	42	2.5×10^{-4}	2

grain size and specific surface area of minerals, specified in reactive transport modeling, are determined based on the sieve test of the crushed rocks.

The geofluid chemistry data used in the TOUGHREACT simulator is provided in Table 4. The geofluid used for the batch reactor experiments was taken from the field. During batch reactor experiments, geofluid samples are regularly taken for analysis. The measured data is recalculated with the PHREEQC at the corresponding P-T conditions.

The modeling workflow begins with the natural-state simulations until reaching plausible P-T and the partial pressure of CO_2 results fitted to the static measurements ignoring the reactive transport. Afterward, the wells in the localized model region commenced production and injection in February 2013 (the beginning of the dynamic model); thus, reactive transport is enabled. Note that each well in this region commences on different dates, and some of the wells turn from production to injection or vice versa. For instance, the well-D_{inj} was used as an injection well between 2013 and 2017, but it has been idle since 2018. The well-G_{inj} was used for production in 2017 for a

couple of months; however, it is converted to an injection well beginning on October 2018. Later, it is used as a pilot injection well for fluid-CO_2 injection on Oct 2022. To compare the impact of the CO_2 injection, the reactive transport simulations are performed with the effluent geofluid-CO_2 injection case and the effluent geofluid injection without a CO_2 mixture.

5. Results

The static P-T of the wells and the history match of the CO_2 mass fraction in the localized numerical model are fitted to the measured values. Figure 3 shows the saturation indices of minerals of muscovite-schist and quartz-schist, respectively. The detailed comparison results can be found elsewhere (GECO 2020, 2023). The effluent geofluid injection from the well-G_{inj} began in October 2018, and the mixture of effluent geofluid and CO_2 started in October 2022 in the model. Figure 4 demonstrates a comparison of the geochemical interaction process in the vicinity of well-G_{inj} over time for the muscovite schist scenario. The results represent geochemical reactions of the injected

Table 4. Calculated geofluid chemistry for deep reservoir and surface-line conditions of the wells. [a] Ambient temperature. [b] calculated pH of the geofluid at the corresponding temperature with the PHREEQC program. The initial reservoir geofluid chemistry is equilibrated with 3% of the CO_2 weight fraction.

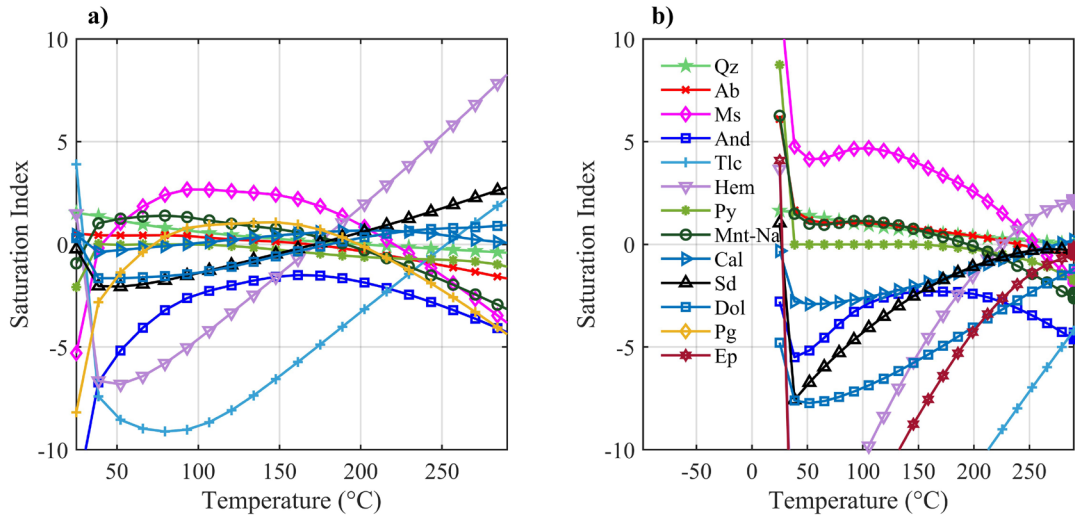| Parameter	Reservoir	Injected geofluid at Well-G_{inj}
T-pH (°C)	220 [a]	105 [a]
pH	6.5 [b]	8.86 [b]
Primary Species	Amount mol kg^{-1}	
Al^{+3-}	1×10^{-25}	5.2×10^{-24}
Br^-	1.3×10^{-5}	1.65×10^{-5}
Ca^{+2}	4.5×10^{-5}	4.77×10^{-5}
Cl^-	3.9×10^{-3}	4.68×10^{-3}
F^-	1.2×10^{-3}	1.5×10^{-3}
Fe^{+2}	1.43×10^{-7}	2.46×10^{-8}
H^+	3.16×10^{-7}	1.64×10^{-9}
HCO_3^-	0.0943	2.86×10^{-3}
K^+	4.53×10^{-3}	6.07×10^{-3}
Mg^{+2}	1.22×10^{-6}	4.71×10^{-7}
Mn^{+2}	4.93×10^{-8}	2.49×10^{-7}
Na^+	0.0487	0.0678
$SiO_{2(aq)}$	1.9×10^{-3}	1.1×10^{-3}

Figure 3. Saturation indices of minerals; a) Muscovite-schist, b) Quartz-schist.

geofluid at a depth of approximately 2313 m flowing from the perforated portion of the well-G_{inj} to the flow path in the model (e.g., the center of the grid, the grid size 255 m², 5×10^4 m³).

The plots on the left-hand side (a, c, and e) show the results of the effluent geofluid-CO_2, whereas the plots in Figure 4 on the right-hand side (b, d, and f) depict the

outcomes without a CO_2 mixture. As the effluent injection begins, the temperature in the corresponding grid decreases from 220 °C to 105 °C and reaches a steady state in terms of enthalpy within a short period (e.g., a couple of days).

The saturation indices of minerals shown in Figure 3 indicate possible secondary mineral precipitation. For the calculation of saturation indices with PHREEQC,
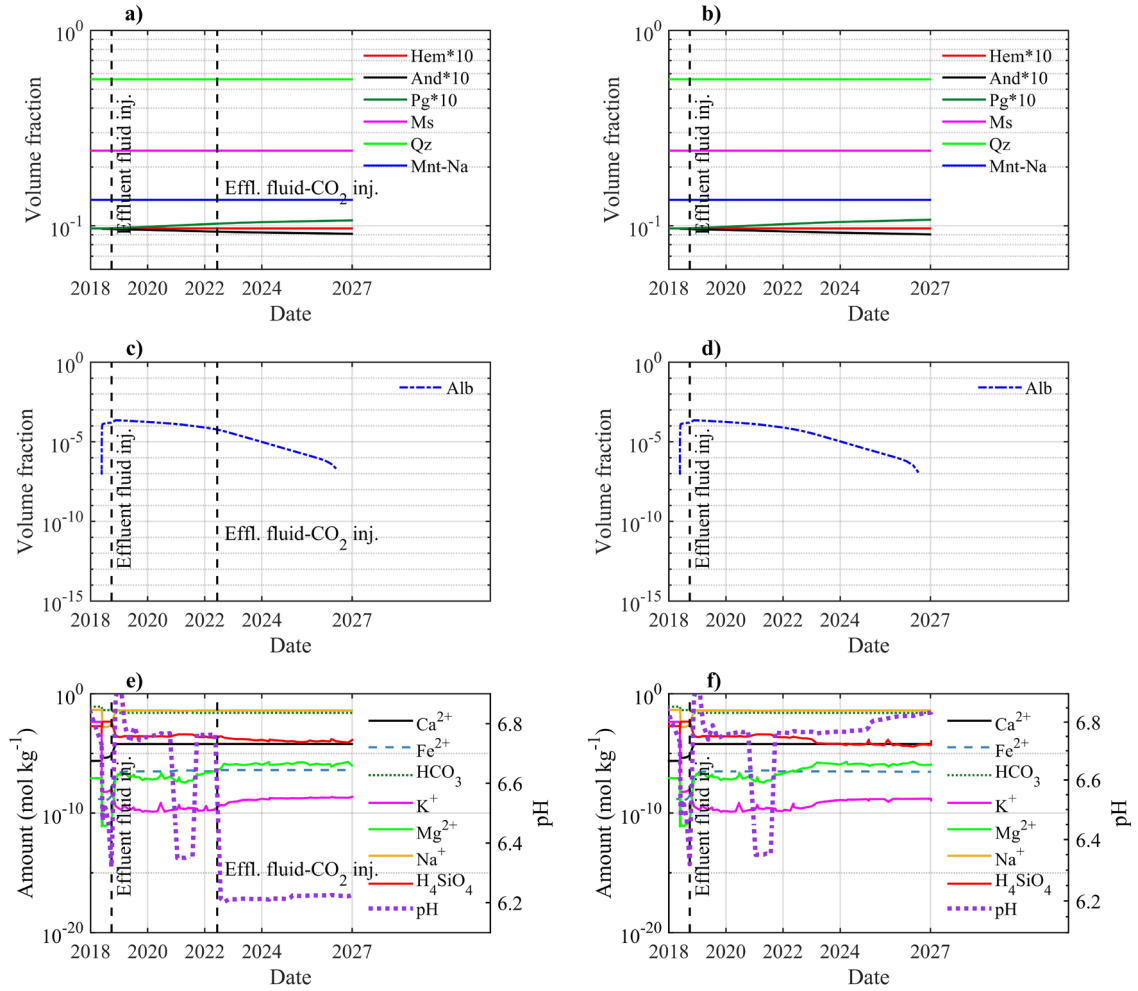
Figure 4. Muscovite schist scenario results over time at a depth of 2313 m for the well-G$_{inj}$. Plots **a, c,** and **e** depict the results with effluent geofluid-CO$_2$ injection taking place in October 2022, whereas plots **b, d**, and **f** show the results only the continuous effluent geofluid injection without CO$_2$ mixture. **a** and **b)** Primary mineral assemblage; **c** and **d)** secondary minerals; **e** and **f)** aqueous species and the pH. Except for albite, other specified secondary minerals, given in Table 2, are not observed.

we linearly increased the partial pressure of CO$_2$ as the temperature rises in the system representing the injection (105 °C) and reservoir conditions (220 °C).

We compared the experimentally evaluated mineral phases with the PHREEQC results. At the injection temperature of around 105 °C, paragonite can be more dominant than andalusite at lower temperatures, and albite mineral can be observed as a secondary mineral for muscovite-schist. Calcite, dolomite, siderite, and talc are undersaturated below 200 °C indicating that these minerals may not be precipitated in the system during the injection. For quartz-schist under injection conditions, albite and montmorillonite-Na are supersaturated below 200 °C, and andalusite is again undersaturated. This may

indicate that andalusite may not be a constituent of the schist at reservoir conditions, as found in EDX analysis in the quartz schist sample (Table 2).

Before the effluent geofluid injection, the albite mineral forms as a secondary mineral in the system (Figures 4c and 4d). The samples are taken from the outcrops, and montmorillonite-Na is a weathering product of albite at atmospheric conditions (Coetsiers and Walraevens 2006). Therefore, Na-bearing aluminosilicate minerals such as montmorillonite-Na may transform to albite in small amounts in this reservoir system.

According to Velde (1977), in Al-Si-bearing metamorphics one mineral can exchange ions with another mineral to form different phases, for instance, andalusite

to paragonite. If the major chemical components Na, Al, and SiO_2 are perfectly mobile in the fluid system their amount determines the phases formed under constant P-T conditions. Based on this approach, albite, and andalusite minerals react to form paragonite after the injection (Figures 4a and 4c). The possible reaction occurring in this system can be formulated as $NaAlSi_3O_8$ (Albite) + H_2O + Al_2SiO_5 (Andalusite) = $NaAl_3Si_3O_{10}(OH)_2$ (Paragonite) + H_4SiO_4 (Orthosilisic acid). This reaction was experimentally observed belove 200 °C in medium-grade metamorphic rocks with the interaction between paragonite and quartz forming andalusite (Chatterjee 1972). In addition, the saturation index of andalusite shown in Figure 3 also points out that at a temperature below 200 °C, andalusite may dissolve. It can be seen that the injected mixture of CO_2 does not significantly affect the reaction processes compared to the scenario in which the injection does not contain a CO_2 mixture (Figures 4a and 4b). The reason can be accounted for by the small amount of mixed CO_2. A minor impact can be seen only in the pH, which slightly decreases from 6.8 to 6.2 after the effluent geofluid-CO_2 mixture injection.

Figures 5–8 show the 2 kt year^{-1} CO_2 injection results between the pilot injection well-G_{inj} and the nearest production well-E_{pro} at different time frames. Along this flow path, the depth ranges between 2313 m and 2373 m, and the anisotropic permeability varies between 1×10^{-13} m^2 (z-direction) and 3×10^{-12} m^2 (xy-direction). In these figures, the solid line depicts two months before the effluent geofluid injection (Aug 2018); the dashed line shows two months after the effluent geofluid injection (Dec 2018); the point-dashed line describes the results two months after the beginning of the effluent geofluid-CO_2 mixture injection (Dec 2022); the point-line (Apr 2027) demonstrates the results after five years of continuous effluent geofluid-CO_2 mixture injection.

Figure 5 shows the variations in the CO_2 trends at a depth between 2000 m and 2200 m. The exported data are taken from the blocks having different elevations. Therefore, the initial mass fraction of CO_2 in Figure 5a exhibit fluctuation. The decrease in the CO_2 near the well-E_{pro} cannot be explained by CO_2 mineralization as any secondary carbonate minerals have not been observed. As the injection commenced in well-G_{inj}, the geofluid front moves mostly toward well-E_{pro} where it dilutes the CO_2 concentration. The significant production rates in the domain also contribute to the decline of CO_2 over time. On the other hand, the injected CO_2 amount (2 kt year^{-1}) provides a slight recovery
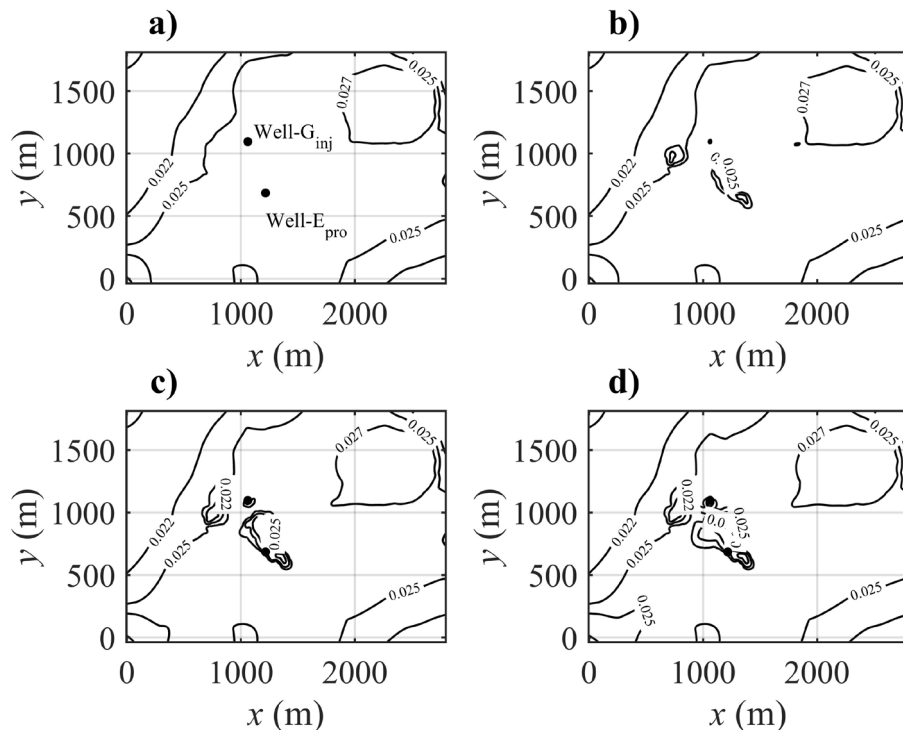

Figure 5. The change in $CO_{2(liq)}$ mass fraction in the mean reservoir depth (2200 m) over time. **a)** Initial $CO_{2(liq)}$ mass fraction in the reservoir before the wells commence (Feb 2013); **b)** two months after well-G_{inj} begins only geofluid injection (Dec 2018); **c)** two months after the beginning of the effluent geofluid-CO_2 mixture injection (Dec 2022); **d)** after five years of continuous effluent geofluid-CO_2 mixture injection (Apr 2027).

for the partial pressure of CO_2 in the reservoir in a long-term injection while avoiding the gaseous phase. The increased Ca^{2+}, Fe^{2+}, and Mg^{2+} over time, shown in Figure 6a, indicates that the injected geofluid changes the geofluid chemistry along the flow path. This triggers some dissolution reactions of other minerals such as montmorillonite and hematite.

Figure 7a demonstrates that the andalusite-paragonite reaction occurs near the injection well over time, and its reactivity decreases over distance. As the secondary mineral, albite forms along this flow path, and its amount increases in time. Other defined secondary minerals are not observed except calcite-formed before the injection (Aug 2018).

The evaluation of results from the quartz schist sample shown in Figures 8a and 8b demonstrates a reaction between andalusite and muscovite similar to the andalusite-

paragonite reaction in the muscovite schist. In addition, albite, paragonite, and montmorillonite-Na are formed as secondary minerals near the injection well-G_{inj}. Moreover, in general, sufficient Fe is mobile, either liberated from Fe-bearing phases by reaction or from the geofluid to stabilize minerals containing Na. According to Velde (1977), the dioctahedral and trioctahedral expanding species can complete a stable solid solution with various possible exchangeable interlayer ions in hydrothermal systems below 250 °C. In the vicinity of well-G_{inj}, intergrowths of Na-K micas likely form montmorillonite-Na as a solid solution interlaying of these two types of mineral structures that could be muscovite-paragonite.

Figure 9 demonstrates that calcite does not show a typical dissolution/precipitation behavior concerning the
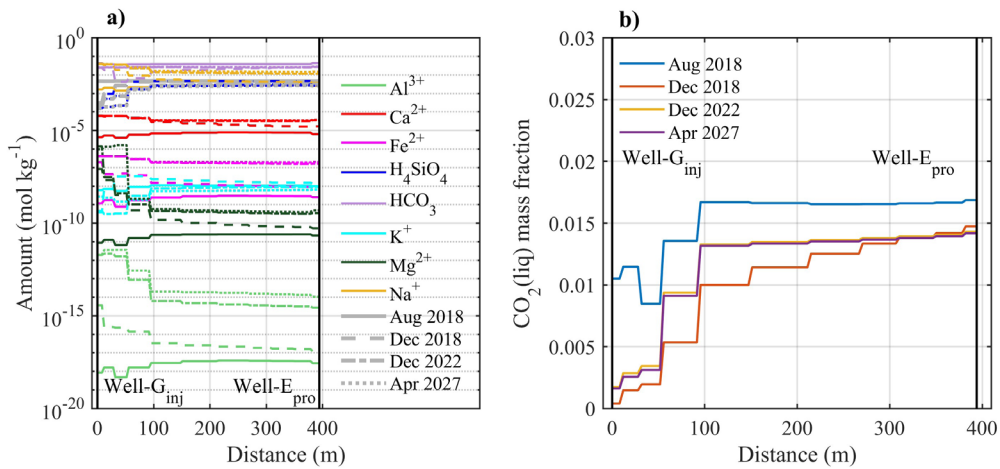

Figure 6. Muscovite schist scenario results over the distance between well-G_{inj} and well-E_{pro}. **a)** Aqueous species over distance at different times; **b)** $CO_{2(liq)}$ mass fraction to the geofluid mass.
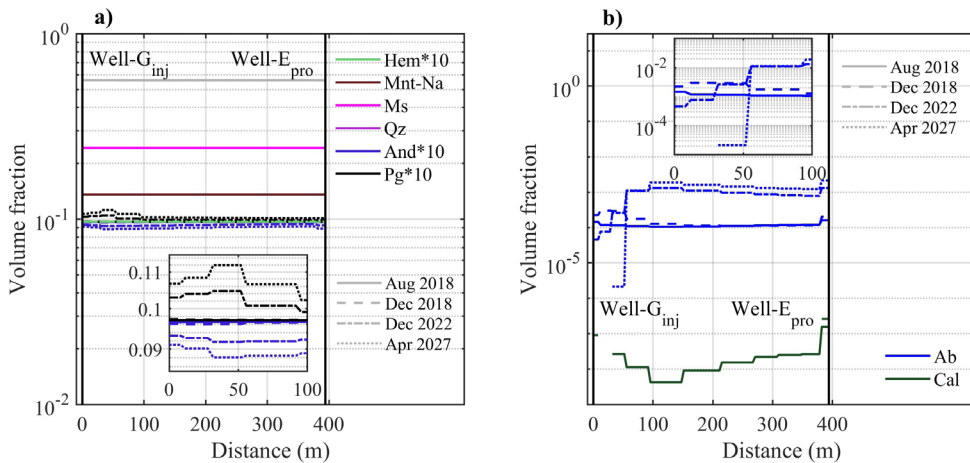

Figure 7. Muscovite schist scenario results over the distance between well-G_{inj} and well-E_{pro}. **a)** Aqueous species over distance at different times; b) $CO_{2(liq)}$ mass fraction to the geofluid mass. Only albite and calcite are observed as secondary minerals along the flow path and the albite amount only increased over time.

temperature. At a temperature around 105–150 °C, calcite precipitation can be expected near well-G_{inj} (Figure 9b). However, calcite does not form around the well-G_{inj}, but it precipitates as the temperature rises close to the well-E_{pro}. Epidote mineral likely prevents carbonization as Ca^{2+} ions that can capture CO_2 as calcite close to the injection where the temperature is below 200 °C. On the other hand, as the temperature and the CO_2 amount are larger in the reservoir along the flow path toward the well-E_{pro}, epidote cannot dominate the system anymore, and calcite forms.

6. Discussion
In the evaluations of XRD measurements, the margin of error is high in those with a quantitative abundance of minerals in the rock samples below 3%. It is also difficult

to clearly distinguish between muscovite and paragonite in thin-section analysis enough to estimate their relative quantities. This may slightly affect the interpretation of the results.

In muscovite schist and quartz schist samples, Na-bearing minerals were observed before the batch experiment. A solid solution series is a compositional range between end-member minerals that has the same basic chemical formula. The solid solution minerals are likely forming and/or adjusting their compositions to take some ions, such as Na, from the geofluid.

The geochemical reaction evaluations with PHREEQC and TOUGHREACT programs which are developed based on the law of mass action approach, typically do not deal with solid solutions. Some newly improved databases,
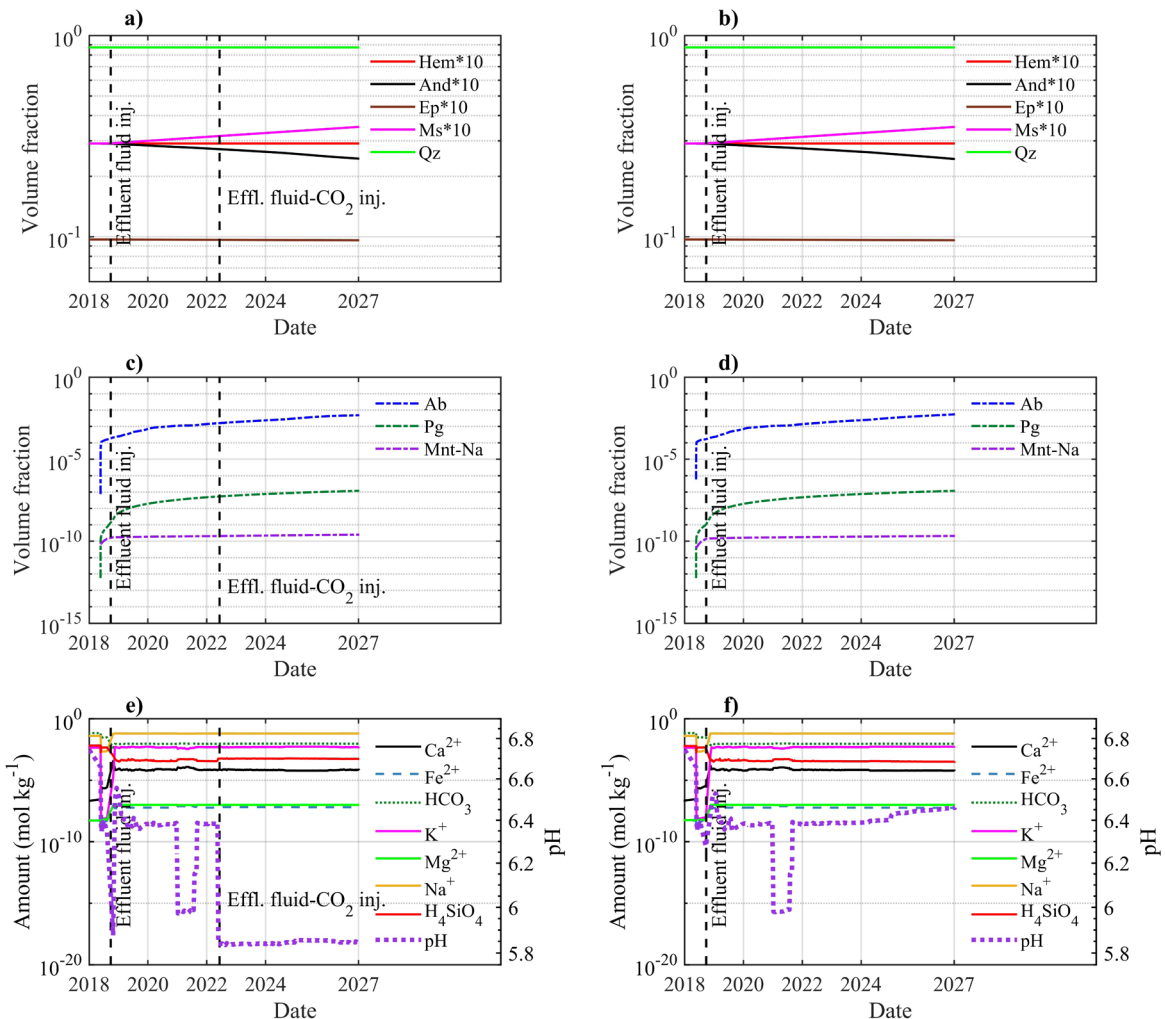

Figure 8. Quartz schist scenario results over time at a depth of 2313 m for the well-G_{inj}. Plots **a**, **c**, and **e** depict the results with effluent geofluid-CO_2 injection taking place in October 2022, whereas plots **b**, **d**, and **f** show the results of only the continuous effluent geofluid injection without CO_2 mixture. **a** and **b**) Primary mineral assemblage; **c** and **d**) secondary minerals; **e** and **f**) aqueous species and the pH. Except for albite, paragonite, and montmorillonite-Na, other specified secondary minerals, given in Table 2, are not observed.
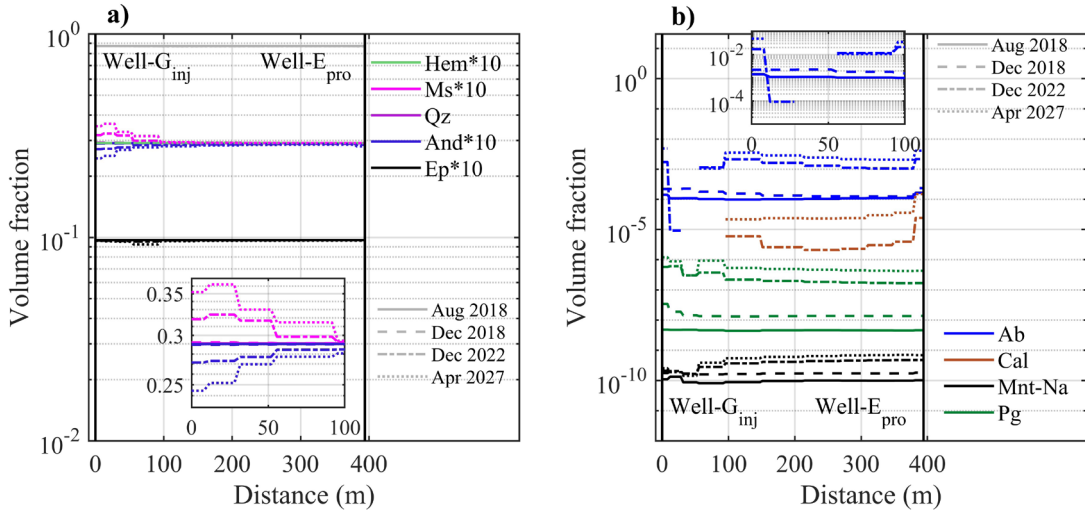
Figure 9. Quartz schist scenario results over the distance between well-G_{inj} and well-E_{pro}. **a)** Aqueous species over distance at different times; **b)** $CO_{2(liq)}$ mass fraction to the geofluid mass. Albite, calcite, montmorillonite-Na, and paragonite are observed along the flow path, and their amount increases over time.

such as Thermoddem, can help to achieve reliable results concerning the end-members of minerals for metamorphic rocks.

Gibbs Energy Minimization (GEM)-Selector program developed by the Paul Scherrer Institut, in theory, can model solid solutions (Kulik et al., 2013). However, its thermodynamic databases for metamorphic rocks are currently limited.

7. Conclusion

Reactive transport simulations are carried out based on the updated field evaluations for the Kızıldere geothermal reservoir. The aim is to reduce the uncertainty in terms of the mineralogy of the rocks, the anisotropic permeability, and the connectivity between the wells. Moreover, different thermodynamic databases are tested. According to the previous and current analyses, to keep the injection stable as a single-phase, the maximum mixture amount of CO_2 is 0.057 moles per kg of water (at 105 °C, 0.25 wt% of the injected effluent geofluid). In this study, five years of continuous effluent geofluid-CO_2 mixture injection at around 105 °C corresponding to 2 kt year^{-1} of CO_2 injection is considered.

Muscovite schist and quartz schist are analyzed. The chemical system is mostly dominated by K-Na-A1-Si-related ions. The amount of other cations which are more suitable to form carbonate minerals with the CO_2, such as Ca^{2+}, Fe^{2+}, and Mg^{2+}, are small in the system, and they are consumed by mica and clay minerals in the reactions to form end-members of these phyllosilicates. Moreover, the existence of mica and alkali minerals triggers the formation of solid solutions in these metamorphic rocks.

The Thermoddem thermodynamic database provides more consistent results concerning the solid solutions and end-members of minerals with regards to the experimental analysis and field observations, compared to the EQ3/6 v7.2b database used by default by TOUGHREACT (Wolery, 1992). Some other modeling approaches for geochemical systems using the Gibbs energy minimization method may support more reliable results for solid solution reactions as long as the database is appropriate for metamorphic rocks.

The CO_2 injection process is convenient under the admissible mixture and temperature ranges that keep the injection remain stable as a single phase. The injected CO_2 is captured as the solubility-trapping form and transported as aqueous bicarbonate. The mineralization of CO_2 is limited. The primary reason can be the small amount of divalent cations Ca^{2+}, Fe^{2+}, and Mg^{2+} in this chemical system, and their interaction is mainly controlled by the K-A1-Si-bearing-minerals, such as muscovite, producing end-members as paragonite. The higher CO_2 content in the reservoir, the pH, and the coexisting geofluid-rock-CO_2 interactions can be considered minor factors affecting the carbonization process. On the other hand, this study demonstrated that the mitigation process of CO_2 emission is successful with solubility-trapping in a geothermal system. In the Kızıldere field, more than ten wells have been used for the effluent geofluid injection and considering 2 kt year^{-1} of CO_2 mixture for each well, approximately more than 200 kt of CO_2 in ten years can be safely injected into the geothermal reservoir. This also harnesses the partial pressure of CO_2 reducing the energy consumption of the pumps to extract the geofluid from the reservoir and sustaining production for the long term.

References

Alçiçek H, Varol B, Özkul M (2007). Sedimentary facies, depositional environments and palaeogeographic evolution of the Neogene Denizli Basin, SW Anatolia, Turkey.

Sedimentary Geology 202: 596–637. https://doi.org/10.1016/j.sedgeo.2007.06.002

Aradóttir ESP, Sonnethal EL, Björnsson G, Johnsson H (2012). Multidimensional reactive transport modeling of CO_2 mineral sequestration in basalts at the Hellisheidi geothermal field, Iceland. International Journal of Greenhouse Gas Control 9: 24-40. https://doi.org/10.1016/j.ijggc.2012.02.006

Battistelli A, Calore C, Pruess K (1997). The simulator TOUGH2/EWASG for modelling geothermal reservoirs with brines and non-condensible gas. Geothermics 26 (4): 437–464. https://doi.org/10.1016/S0375-6505(97)00007-2

Berndsen M, Nehler M, Nardini I, Erstling S, Saenger EH et al. (2022). Experimental study on rock-CO_2 interaction processes at HP/HT conditions. In: European Geothermal Congress (EGC) 17-21 October 2022, Berlin, Germany.

Blanc Ph, Lassin A, Piantone P, Azaroual M, Jacquemet N et al. (2012). Thermoddem: A geochemical database focused on low temperature water/rock interactions and waste materials. Applied Geochemistry 27 (10): 2107-2116. https://doi.org/10.1016/j.apgeochem.2012.06.002

Blasco M, Gimeno MJ, Auque LF (2017). Comparison of different thermodynamic databases used in a geothermometrical modelling calculation. Procedia Earth and Planetary Science 17: 120 – 123. https://doi.org/10.1016/j.proeps.2016.12.023

Chatterjee ND (1972). The Upper Stability Limit of the Assemblage Paragonite + Quartz and Its Natural Occurrences. Contributions to Mineralogy and Petrology 34: 288-303. ttps://doi.org/10.1007/BF00373759

Clark DE, Oelkers EH, Gunnarsson I, Sigfússon B, Snæbjörnsdóttir SÓ et al. (2020). CarbFix2: CO_2 and H_2S mineralization during 3.5 years of continuous injection into basaltic rocks at more than 250 °C. Geochimica et Cosmochimica Acta 279: 45-66. https://doi.org/10.1016/j.gca.2020.03.039

Coetsiers M, Walraevens K (2006). Chemical characterization of the Neogene Aquifer, Belgium. Hydrogeology Journal 14: 1556–1568. https://doi.org/10.1007/s10040-006-0053-0.

Erol S, Akın T, Başer A, Saraçoğlu Ö, Akın S (2022a). Geofluid-CO_2 injection impact in a geothermal reservoir: Evaluation with 3-D reactive transport modeling. Geothermics 98: 102271. https://doi.org/10.1016/j.geothermics.2021.102271

Erol S, Bayer P, Akın T, Akın S (2022b). Advanced workflow for multi-well tracer test analysis in a geothermal reservoir. Geothermics 101: 102375. https://doi.org/10.1016/j.geothermics.2022.102375

Galeczka IM, Stefánsson A, Kleine BI, Gunnarsson-Robin J, Snæbjörnsdóttir SÓ et al. (2022). A pre-injection assessment of CO_2 and H_2S mineralization reactions at the Nesjavellir (Iceland) geothermal storage site. International Journal of Greenhouse Gas Control 115: 103610. https://doi.org/10.1016/j.ijggc.2022.103610

GECO (2020). Report: Deliverable 2.9 Report on Integrated Geological and Reservoir Models and Injection Modelling. https://geco-h2020.eu/deliverables/

GECO (2023). Report: Deliverable 7.4 Report on Models updated and processes optimized in the light of the first results (in the preparation process). https://geco-h2020.eu/deliverables/

Gunnarsson I, Aradóttir ES, Oelkers EH, Clark DE, Arnarson MÞ et al. (2018). The rapid and cost-effective capture and subsurface mineral storage of carbon and sulfur at the CarbFix2 site. International Journal of Greenhouse Gas Control 79: 117-126. https://doi.org/10.1016/j.ijggc.2018.08.014

Kulik DA, Wagner T, Dmytrieva SV, Kosakowski G, Hingerl FF et al. (2013). GEM-Selektor geochemical modeling package: revised algorithm and GEMS3K numerical kernel for coupled simulation codes. Computational Geosciences 17: 1-24. https://doi.org/10.1007/s10596-012-9310-6

Palandri JL, Kharaka YK (2004). A compilation of rate parameters of water-mineral interaction kinetics for application to geochemical modeling. USGS report 2004-1068. U.S. Geological Survey. Menlo Park, CA-USA.

Parkhurst DL, Appelo CAJ (2013). Description of input and examples for PHREEQC version 3 a computer program for speciation, batch-reaction, one-dimensional transport, and inverse geochemical calculations. U.S. Geological Survey Techniques and Methods. Amsterdam, Netherlands. https://pubs.usgs.gov/tm/06/a43/

PerkinElmer (2010). Software Guide: WinLab32 for ICP instrument control software. PerkinElmer Inc. Waltham, MA-USA.

Pruess K, Oldenburg CM, Moridis GJ (1999). TOUGH2 User's Guide, Version 2.0, Lawrence Berkeley National Laboratory, Report LBNL-43134, Berkeley, CA-USA.

Ratouis TMP, Snæbjörnsdóttir SO, Sigfússon B, Gunnarsson I, Voigt MJ et al. (2021). Reactive transport model of CO_2 and H_2S mineral sequestration at the CarbFix2 reinjection site, Hellisheiði Geothermal Power Plant, SW-Iceland. In: World Geothermal Congress (WGC) October 24-27, Reykjavik, Iceland.

Ratouis TMP, Snæbjörnsdóttir SÓ, Voigt MJ, Sigfússon B, Gunnarsson G et al. (2022). Carbfix 2: A transport model of long-term CO_2 and H_2S injection into basaltic rocks at Hellisheidi, SW-Iceland. International Journal of Greenhouse Gas Control 114: 103586. https://doi.org/10.1016/j.ijggc.2022.103586

Raza A, Glatz G, Gholami R, Mahmoud M, Alafnan S (2022). Carbon mineralization and geological storage of CO_2 in basalt: Mechanisms and technical challenges. Earth-Science Reviews 229: 104036. https://doi.org/10.1016/j.earscirev.2022.104036

Rockware (2022). Graphical interface for the TOUGHREACT v1.2 simulator https://www.rockware.com/product/petrasim/ accessed on 02/8/2022.

Snæbjörnsdóttir SÓ, Gislason SR, Galeczka IM, Oelkers EH (2018). Reaction path modelling of in-situ mineralisation of CO_2 at the CarbFix site at Hellisheidi, SW-Iceland. Geochimica et Cosmochimica Acta 220: 348–366. https://doi.org/10.1016/j.gca.2017.09.053

Şimşek Ş, Yıldırım N, Gülgör A (2004). Developmental and environmental effects of the Kızıldere geothermal power project, Turkey. Geothermics 34: 239–256. https://doi.org/10.1016/j.geothermics.2004.12.005

Snæbjörnsdóttir SÓ, Sigfússon B, Marieni C, Goldberg D, Gislason SR et al. (2020). Carbon dioxide storage through mineral carbonation. Nature Reviews Earth and Environment 1: 90–102. https://doi.org/10.1038/s43017-019-0011-8

Stefan C, Neubauer K (2014). White Paper: Single Particle Inductively Coupled Plasma Mass Spectrometry: Understanding How and Why. PerkinElmer Inc., Waltham, MA-USA.

Topçu G, Koç GA, Baba A, Demir MM (2019) The injection of CO_2 to hypersaline geothermal brine: A case study for Tuzla region. Geothermics 80: 86-91. https://doi:10.1016/j.geothermics.2019.02.011

TOUGHREACT (2022). Multiphase reactive-transport code based on TOUGH2 simulator. https://tough.lbl.gov/software/toughreact/ accessed on 02/8/2022.

Velde B (1977). Clays and Clay Minerals in Natural and Synthetic Systems. Developments in sedimentology 21, 1st Edition. Amsterdam, Netherlands. ISBN: 9780080869339.

Whitney DL, Evans BW (2010). Abbreviations for names of rock-forming minerals. American Mineralogist, 95(1): 185-187. https://doi.org/10.2138/am.2010.3371

Wolery TJ (1992). EQ3/6: Software package for geochemical modeling of aqueous systems: Package overview and installation guide (version 8.0), Lawrence Livermore National Laboratory Report UCRL-MA-110662 PT I, Livermore, CA-USA.

Xu T, Sonnenthal E, Spycher N, Pruess K (2008). TOUGHREACT User's Guide: A Simulation Program for Non-isothermal Multiphase Reactive Transport in Variably Saturated Geologic Media, version 1.2.1. Report LBNL-55460-2008., Lawrence Berkeley National Laboratory. Berkeley, CA-USA.

Appendix A

A summary of the primary and secondary phases used in the reaction transport simulations is given:

Quartz: $SiO_2 = SiO_2$ (1)

Muscovite: $KAl_2(Si_3Al)O_{10}(OH)_2 + 10H^+ = 3Al^{+3} + 3SiO_2 + 6H_2O + K$ (2)

Albite: $NaAlSi_3O_8 + 4H^+ = Na^+ + Al^{+3} + 3SiO_2 + 2H_2O$ (3)

Hematite: $Fe_2O_3 + 6H^+ = 2Fe^{+3} + 3H_2O$ (4)

Calcite: $CaCO_3 + H^+ = Ca^{+2} + HCO_3^-$ (5)

Siderite: $FeCO_3 + H^+ = Fe^{+2} + HCO_3^-$ (6)

Pyrite: $FeS_2 + H_2O = 0.25H+ + 0.25SO_4^{-2} + Fe^{+2} + 1.75HS$ (7)

Montmorillonite-Na: $Na_{0.35}Mg_{0.35}Al_{1.65}Si_4O_{10}(OH)_2 + 6H^+ = 0.175Ca^{+2} + 1.65Al^{+3} + 0.35Mg^{+2} + 4SiO_2 + 4H_2O$ (8)

Epidote: $Ca_2FeAl_2Si_3O_{12}OH + 13H^+ = Fe^{+3} + 2Al^{+3} + 2Ca^{+2} + 3SiO_2 + 7H_2O$ (9)